EFDA–JET–CP(11)04/01

P. Buratti, M. Baruzzo, R.J. Buttery, C.D. Challis, I.T. Chapman, F. Crisanti, L. Figini, M. Gryaznevich, H. Han, T.C. Hender, J. Hobirk, D.F. Howell, F. Imbeaux, E. Joffrin, O.J. Kwon, X. Litaudon, P. Maget, J. Mailloux and JET EFDA contributors

Onset of Tearing Modes in JET Advanced Scenarios

Onset of Tearing Modes in JET Advanced Scenarios

P. Buratti[1], M. Baruzzo[2], R.J. Buttery[3], C.D. Challis[4], I.T. Chapman[5], F. Crisanti[1], L. Figini[5], M. Gryaznevich[4], H. Han[6], T.C. Hender[4], J. Hobirk[7], D.F. Howell[4], F. Imbeaux[8], E. Joffrin[8], O.J. Kwon[9], X. Litaudon[8], P. Maget[8], J. Mailloux[4] and JET EFDA contributors*

JET-EFDA, Culham Science Centre, OX14 3DB, Abingdon, UK

[1]Associazione EURATOM-ENEA sulla Fusione, C.R. Frascati, Roma, Italy
[2]Associazione EURATOM-ENEA sulla Fusione, Consorzio RFX Padova, Italy
[3]General Atomics, San Diego, CA, USA
[4]EURATOM-CCFE Fusion Association, Culham Science Centre, OX14 3DB, Abingdon, OXON, UK
[5]Associazione EURATOM-ENEA sulla Fusione, IFP Milano, Italy
[6]Department of Nuclear Engineering, Seoul National University, Seoul 151-742 Korea
[7]Max-Planck-Institut für Plasmaphysik, Garching, Germany, Euratom Assoziation
[8]CEA, IRFM, F-13108 Saint Paul-lez-Durance, France
[9]Department of Physics, Daegu University, Gyeongbuk 712-714 Korea
** See annex of F. Romanelli et al, "Overview of JET Results", (23rd IAEA Fusion Energy Conference, Daejon, Republic of Korea (2010)).*

Preprint of Paper to be submitted for publication in Proceedings of the
38th EPS Conference on Plasma Physics
Strasbourg, France
(27th June 2011 - 1st July 2011)

“This document is intended for publication in the open literature. It is made available on the understanding that it may not be further circulated and extracts or references may not be published prior to publication of the original when applicable, or without the consent of the Publications Officer, EFDA, Culham Science Centre, Abingdon, Oxon, OX14 3DB, UK.”

“Enquiries about Copyright and reproduction should be addressed to the Publications Officer, EFDA, Culham Science Centre, Abingdon, Oxon, OX14 3DB, UK.”

The contents of this preprint and all other JET EFDA Preprints and Conference Papers are available to view online free at www.iop.org/Jet. This site has full search facilities and e-mail alert options. The diagrams contained within the PDFs on this site are hyperlinked from the year 1996 onwards.

ABSTRACT

One main limitation to the performance of high-β_N tokamak regimes arises from the development of tearing modes that short-circuit radial transport by forming magnetic islands. The observation of such modes in linearly stable plasmas led to the concept of Neoclassical Tearing Modes (NTM), which are driven by the perturbed bootstrap current if an external event produces a seed island overcoming a metastability threshold.

Magnetic islands that form in consequence of the development of long-lasting kink modes are considered in this paper. Kink modes that grow on long time-scales (typically 0.2 s from birth to saturation) have been systematically studied at JET [1] since they constitute the main obstacle to the prolongation of high β_N phases at high confinement in the steady-state advanced regime. The mode topology transforms from kink to tearing after a period that will be referred to as island latency. Attention will be focused on a case with long latency period, which is particularly challenging in view of the comparison with the rapid seed island formation that is observed at large sawtooth crashes.

1. TRANSITION FROM KINK TO TEARING MODE TOPOLOGY

In previous works [1, 2, 3] the mode topology has been inferred from spectral cross-phase analysis of temperature oscillations, under the assumption that temperature contours move in phase with flux contours. In the example shown in fig. 1 the island marker (i.e. a π-jump in the phase difference between two adjacent ECE channels) appears after 250ms of mode growth. The plasma scenario is of the steady-state type [4], with $\beta_N = 2.65$ and $q_{min} = 1.65$. The mode propagation frequency is close to plasma rotation at the q = 2 radius [1]. The toroidal mode number is n = 1 and the poloidal structure is dominated by the m = 2 component [1]. The analysis presented in fig.1 has the advantage of automatic rejecting both noise and other MHD modes at different frequencies, but it is restricted to the fundamental mode frequency. In order to overcome this limitation, a time-domain approach has been adopted that fully exploits the rich harmonic content of temperature oscillations. A comb filter has been used to recover the rejection properties of the spectral analysis. The comb filter selects the fundamental mode frequency, as given by the FFT of a magnetic coil signal, and its overtone harmonics. FFTs of ECE signals are multiplied by the comb and back-transformed. The number (N) of comb teeth is chosen to keep the overtone harmonics that have good cross-coherence with the magnetic signal. Tooth width is fixed at 11 spectral bins. The application of this technique requires careful selection of analysis windows in which the mode frequency is sufficiently constant and there are no other modes near the comb frequencies. The analysis of seven such windows that have been selected for JET Pulse No: 77877 will be presented in the following. Figure 2 shows some filtered signals for three representative windows, while the corresponding radius-time temperature maps are shown in fig. 3.

The mode starts at t = 6.28s, when a coherent line appears in the spectrogram of the magnetic signal. In fig.3a, at t = 140ms after mode start, temperature contours are distorted but regularly spaced,

which is characteristic of a kink topology. In fig.3b (t = 195ms) an island chain with reconnected regions interleaved by ribbons appears around R = 3.45m. In figure 3c (t = 226ms) a large island appears. In summary, the time-domain analysis reveals that the island forms about 100ms before the appearance of the island marker in the cross-phase; the reason is that the island is initially asymmetric and the temperature perturbation remains in-phase across the plasma. The island width is estimated from the variation of distance between nearby circulating contours. Its evolution is presented in fig. 4. In the following, in order to get a qualitative idea on the current distribution evolution, measured temperature contours are compared with a simple model for flux contours.

2. A SIMPLE QUASI-EQUILIBRIUM MODEL FOR KINK AND TEARING PERTURBATIONS

Since the observed mode evolution is quite slow, inertia is neglected and current is assumed to be a flux function $j = j(\psi)$. A boundary-layer approach is used in which geometry is simplified to a sheared slab with gradients along x and constant background field B_0 along z, while the full non-linearity is retained. Neglecting derivatives in the y (poloidal) direction, integration of $\nabla^2\psi = \mu_0 j_z \equiv J(\psi)$ gives the transverse field $B_y(\psi, y) = \pm\sqrt{2(F(\psi) - G(y))}$. In addition to $J(\psi)$, a current sheet $I_G(y) = 2\sqrt{2(F(\psi_t) - G(y))}$ is present at the turning point $\psi = \psi_t(y)$, where the two branches join. Assuming (without loss of generality) that $\min(\psi_t) = 0$, it follows $(\psi_t) \equiv \psi_s$ that is the amount of reconnected flux. The mode topology is kink for $\psi_s = 0$ and mixed or tearing for $\psi_s > 0$ Flux contour are:

$$r(\psi, y) = r_t(y) \pm \rho(\psi, y), \text{ where } \rho(\psi, y) = \int_{\psi,(y)}^{\psi} \frac{d\psi'}{\sqrt{2\,(F(\psi') - G(y))}} \text{ and } F(\psi) = \int_0^{\psi} J(\psi')d\psi'.$$

This well-known scheme has been used for non-linear studies on ideal [5] and fast-reconnecting [6] modes, in which general properties of $F(\psi)$ and $G(\theta)$ were found by means of variational principles. The approach is much simpler here. A "current groove" shape is assumed, with $J = J_{in}$ for $\psi \le \psi_1$ and $J = J_{out}$ for $\psi > \psi_1$. The current sheet becomes $I_G(y) = 2J_{in}\,g(y)$, where $g(y) = \sqrt{2\psi_t/J_{in} - 2G/J_{in}^2}$ and the odd part of displacement $\rho = \sqrt{\hat{\psi} - \hat{\psi}_t + g^2} - g$ for $\hat{\psi}_t \le \hat{\psi}_t$ and

$\rho = \sqrt{1-a}\ \sqrt{\hat{\psi} - a\hat{\psi}_1 + (1-a)(g^2 - \hat{\psi}_t)} + a\sqrt{\hat{\psi}_1 - \hat{\psi}_t + g^2} - g$ for $\hat{\psi} > \hat{\psi}_1$, where $a = 1 - J_{in}/J_{out}$ is the groove depth and $\hat{\psi} = 2\psi/J_{in}$ are fluxes in square length units. Boundary conditions on flux contour oscillations are $\xi \to \xi_{\pm}(y)$ for $r \to \pm\infty$. In terms of mean and differential displacement, $\bar{\xi}(y) = (\xi_+ + \xi_-)/2$ and $\tilde{\xi}(y) = (\xi_- - \xi_+)/2$, we have $r_t(y) = \bar{\xi}(y)$ and $g(y) = \left(\tilde{\xi} + a\sqrt{\tilde{\xi}^2 + (1-a^2)(\hat{\psi}_1 - \hat{\psi}_t)}\right)/(1-a^2)$. The total current perturbation resulting from the current sheet and from the groove is $\Delta I = 2J_{out}\tilde{\xi}$.

Simple forms of the free functions are used, $\bar{\xi}(y) = \bar{\xi}_m \cos ky$, $\tilde{\xi}(y) = \tilde{\xi}_m \cos ky$, and $\hat{\psi}_t = \hat{\psi}_{tx} \equiv \hat{\psi}_s(1-\cos ky)/2$. This choice gives islands with X-points and five free parameters (a, $\hat{\psi}_1$, $\hat{\psi}_s$, $\bar{\xi}_m$ and $\tilde{\xi}_m$). In addition, Y-points configurations with $\hat{\psi}_t = \hat{\psi}_{tY}(y)$ are considered, where $\hat{\psi}_{tY} = \hat{\psi}_C$ for $\cos ky > -\sqrt{1 - \hat{\psi}_S/\hat{\psi}_1}$ and $\hat{\psi}_{tY} = \hat{\psi}_1(1-\cos^2 ky)$ elsewhere; the additional constraint $a^2\hat{\psi}_1 = \tilde{\xi}_m^2$ applies in this case.

3. COMPARISON BETWEEN THE CURRENT GROOVE MODEL AND EXPERIMENTAL CONFIGURATIONS

The experimental displacement profiles, as obtained by plotting the swing versus the mean position of contours, have a maximum at around mid radius. Comparison with the model (which only gives monotonic profiles) is done in the range on the right side of the maximum, where island formation occurs. For the configuration in fig. 3a $\hat{\psi}_s = 0$ is assumed and the other parameters are varied until the model displacement profile reproduces the experimental one. This gives a pronounced groove depth $a = 0.7$. Model contours overlaid with three experimental ones are shown in fig.5a. Model parameters are annotated in the figure title. No attempt has been done to determine confidence ranges for these parameters; however it is quite clear that in this time slice a substantial current sheet is present at all y. An Y-configuration is used to reproduce data in fig.3b, in which two diverging nearby contours form an oval region. In this case the reconnected flux and the groove depth are determined respectively by horizontal and vertical widths of the oval region, while $\bar{\xi}_m$ and $\tilde{\xi}_m$ result from circulating contours farther away. In this configuration the current groove is shallow ($a = 0.25$) and the current sheet reduces to zero in the reconnected region. Data in fig.3c can be reproduced by an even shallower groove, $a = 0.2$. The X configuration works better than the Y one in this case, although some remnant of the ribbon appears. Also the "in-phase" character of contours in the presence of an island is well reproduced (fig.5c). In summary, the kink configuration is consistent with a deep current groove that implies a substantial current sheet at all *y*. The current groove becomes shallow in reconnected configurations and the current sheet drops to zero around O-points.

DISCUSSION

The comparison between measured and model flux maps indicates that the kink mode develops a current sheet surrounded by a current depression. The island could then be formed by forced reconnection driven by the current sheet. The linear theory of forced reconnection for the collisional, constant-ψ regime gives a characteristic time of the order of the linear tearing time $\tau_c = S^{3/5} \tau_H$ [7], where S is the Lundquist number and τ_H is the local hydromagnetic time scale. The actual value in the island region, $\tau_c \approx 30$ms agrees in order of magnitude with the island latency period. The reconnection time increases by several orders of magnitude with the inclusion of diamagnetic drifts [8], but the latter could be weakened by the pre-existing kink or by non-linear effects.

On the other hand, the 150ms latency period in the presence of a kink perturbation with a dominant resonant (same m = 2) component should be reconciled with rapid formation of m/n = 2/1 or 3/2 seed islands at sufficiently large sawtooth crashes, for which the forcing component is a toroidal sideband of the 1/1 mode or of its 2/2 nonlinear harmonic. A clear difference is that the kink growth time (~70ms) is larger than the Sweet-Parker time (~8 ms) and vice versa for the sawtooth crash. This opposite ordering could give rise to a narrower current sheet structure in the sawtooth case, leading to island formation by current sheet instability rather than by forced reconnection.

ACKNOWLEDGMENT.

This work was supported by EURATOM and carried out within the framework of the European Fusion Development Agreement. The views and opinions expressed herein do not necessarily reflect those of the European Commission.

REFERENCES

[1]. P. Buratti et al., IAEA 20102010 Proc. 23rd Fusion Energy Conf. IAEA-CN-180/EXS/P5-02

[2]. P. Buratti et al., 35th EPS Conf. on Plasma Physics, Crete P1.069 and http://eps2008.iesl.forth.gr/

[3]. P. Buratti et al., 36th EPS Conf. on Plasma Physics, Sofia O2.007 and http://epsppd.epfl.ch/Sofia/start.htm

[4]. J. Mailloux et al 2010 Proc. 23rd Fusion Energy Conf. IAEA-CN-180/EXC/1-4

[5]. M.N. Rosenbluth, R.Y.Dagazian and P.H. Rutherford, Physics of Fluids **16** (1973) 1894

[6]. F.L. Waelbroeck, Phys. Fluids B**1** (1989) 2372

[7]. T.S. Hahm and R.M. Kulsrud, Physics of Fluids **28** (1985) 2412

[8]. R. Fitzpatrick and T.C. Hender, Physics of Fluids B**3** (1991) 644

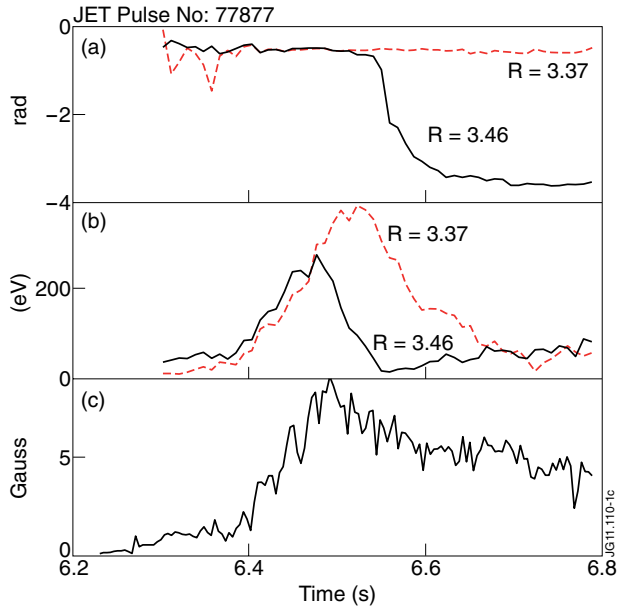

Figure 1: (a) Phase of two ECE channels with respect to a reference magnetic signal. Separation between the two traces at t = 6.55s marks island appearance. (b) Amplitude of temperature oscillations in the same ECE channels. (c) Poloidal field oscillations.

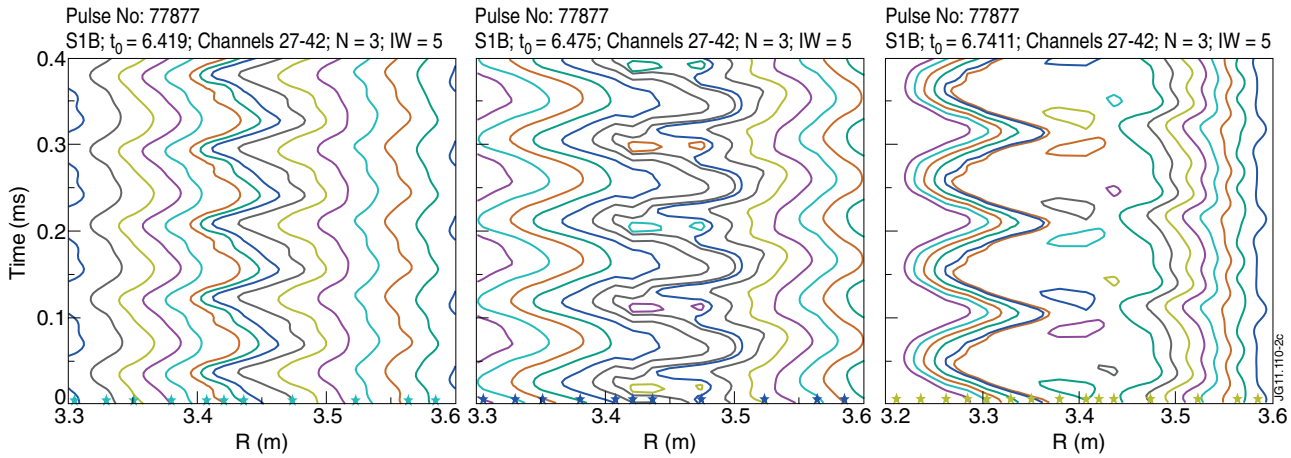

Figure 2: Filtered time traces of some ECE channels in three time slices at 140, 195 and 226 ms after mode start. A few periods are shown from each 10 ms window. The number of harmonics is N = 3.

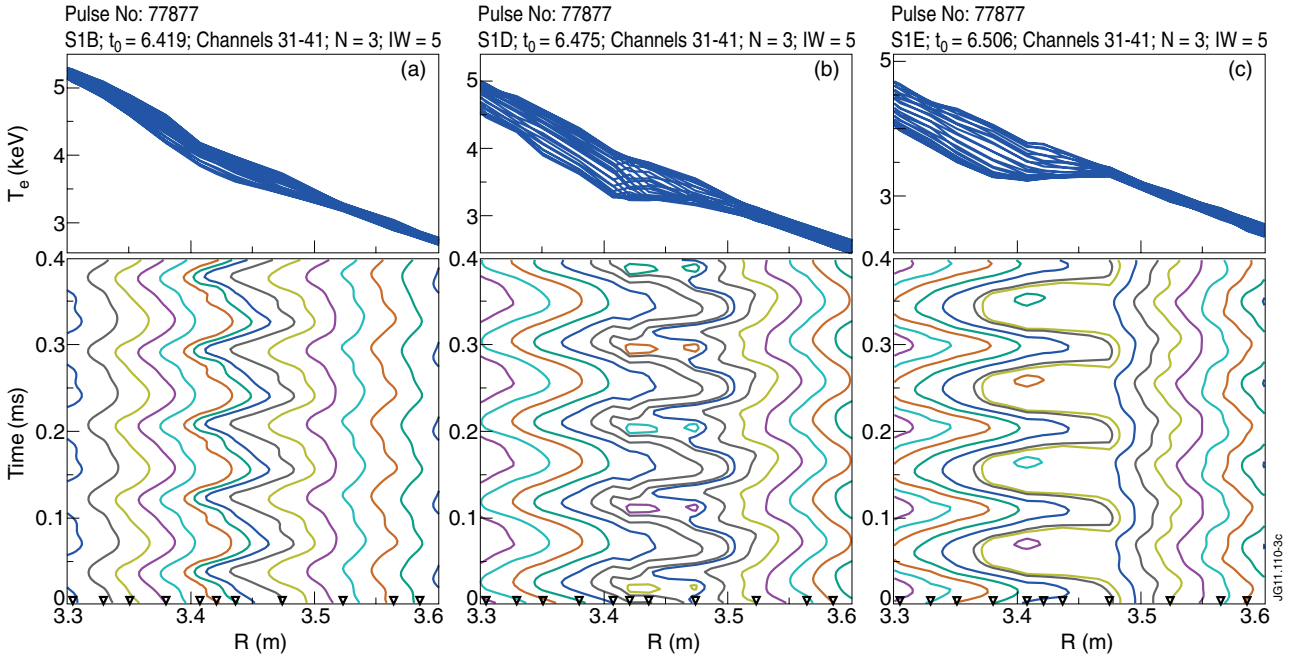

Figure 3: Temperature profiles (upper) and contours (lower) at (a) 140, (b) 195 and (c) 226 ms after mode start. Markers near the horizontal axis indicate actual ECE channels positions.

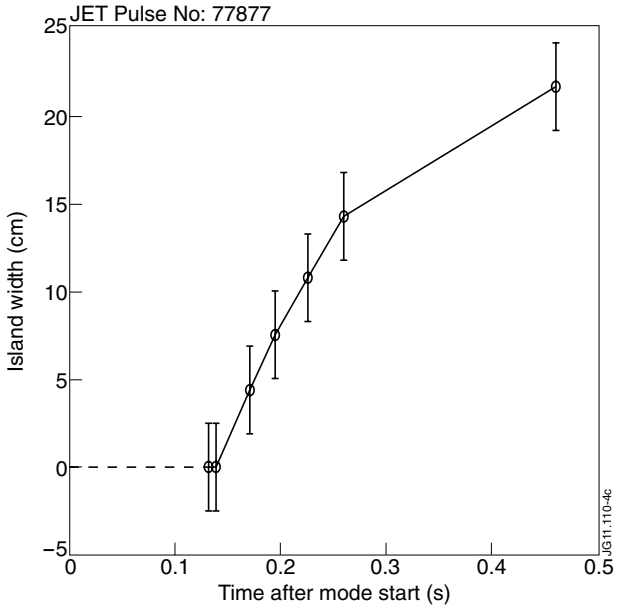

Figure 4: Island width evolution. Error bars correspond to the maximum distance between ECE channels.

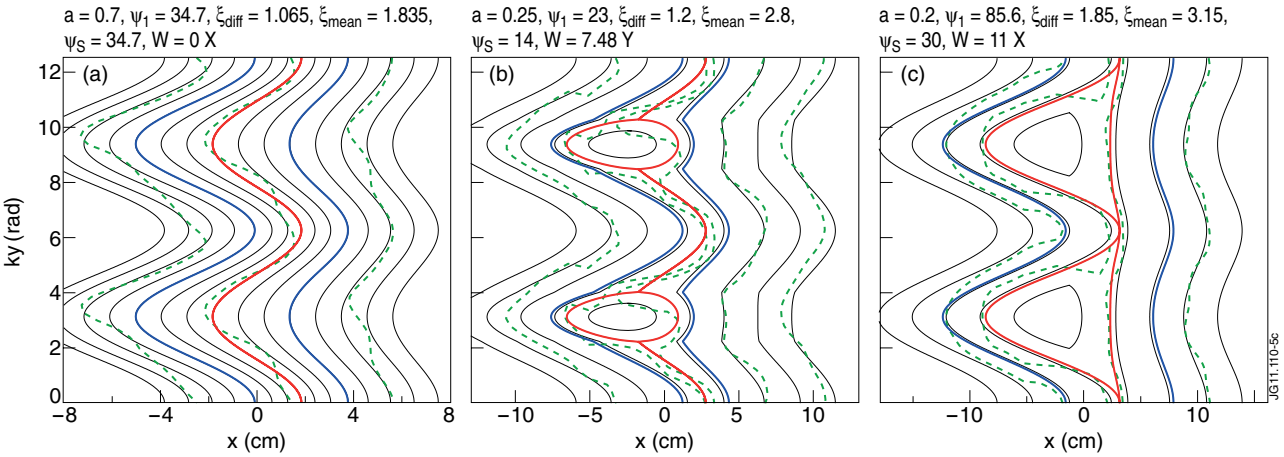

Figure 5: Model flux contours (black), separatrix (red) and current groove edges (blue) for the same times as in fig.3. Dashed green lines show temperature contours shifted in R and rescaled with t = ky/w.